Available online at www.sciencedirect.com
ScienceDirect
Lithos 101 (2008) 435–452
LITHOS
www.elsevier.com/locate/lithos

Refertilization of ancient lithospheric mantle beneath the central North China Craton: Evidence from petrology and geochemistry of peridotite xenoliths

Yan-Jie Tang [a,*], Hong-Fu Zhang [a], Ji-Feng Ying [a], Jin Zhang [a], Xiao-Ming Liu [b]

[a] State Key Laboratory of Lithospheric Evolution, Institute of Geology and Geophysics, Chinese Academy of Sciences, P.O. Box 9825, Beijing 100029, China
[b] State Key Laboratory of Continental Dynamics, Northwest University, Xi'an 710069, China

Received 19 March 2007; accepted 19 September 2007
Available online 2 October 2007

Abstract

The petrology and geochemistry of peridotite xenoliths in the Cenozoic basalts from Fanshi, the central North China Craton (NCC), provide constraints on the evolution of sub-continental lithospheric mantle. These peridotite xenoliths are mainly spinel-facies lherzolites with minor harzburgites. The lherzolites are characterized by low forsterite contents in olivines (Fo<91) and light rare earth element (LREE) enrichments in clinopyroxenes. In contrast, the harzburgites are typified by high-Fo olivines (>91), high-Cr# spinels and clinopyroxenes with low abundances of heavy REE (HREE). These features are similar to those from old refractory lithospheric mantle around the world, and thus interpreted to be relics of old lithospheric mantle. The old lithospheric mantle has been chemically modified by the influx of melts, as evidenced by the Sr–Nd isotopic compositions of clinopyroxenes and relatively lower Fo contents than typical Archean lithospheric mantle (Fo>92.5). The Sr–Nd isotopic compositions of harzburgites are close to EM1-type mantle, and of the lherzolites are similar to bulk silicate earth. The latter could be the result of recent modification of old harzburgites by asthenospheric melt, which is strengthened by fertile compositions of minerals in the lherzolites. Therefore, the isotopic and chemical heterogeneities of the Fanshi peridotite xenoliths reflect the refertilization of ancient refractory lithospheric mantle by massive addition of asthenospheric melts. This may be an important mechanism for the lithospheric evolution beneath the Central NCC.

Keywords: Peridotite xenoliths; Mantle refertilization; Lithospheric mantle; North China Craton

1. Introduction

Asthenosphere–lithosphere and crust–mantle interactions can modify ancient lithospheric mantle roots by the influx of fertile materials (Griffin et al., 1998; Downes, 2001; O'Reilly et al., 2001; Zhang, 2005, Foley et al., 2006; Zhang et al., 2007a). Mantle xenoliths are direct samples of lithospheric mantle fragments, and thus can provide direct information about these mantle processes. Previous studies of mantle xenoliths from the Ordovician diamondiferous kimberlites (Fig. 1) have indicated a thick (>200 km), cold and refractory lithospheric keel beneath the eastern North China Craton (NCC) prior to the Paleozoic, while basalt-borne xenoliths reveal the presence

* Corresponding author. Tel.: +86 10 82998536; fax: +86 10 62010846.
E-mail address: tangyanjie@mail.igcas.ac.cn (Y.-J. Tang).

0024-4937/$ - see front matter © 2007 Elsevier B.V. All rights reserved.
doi:10.1016/j.lithos.2007.09.006

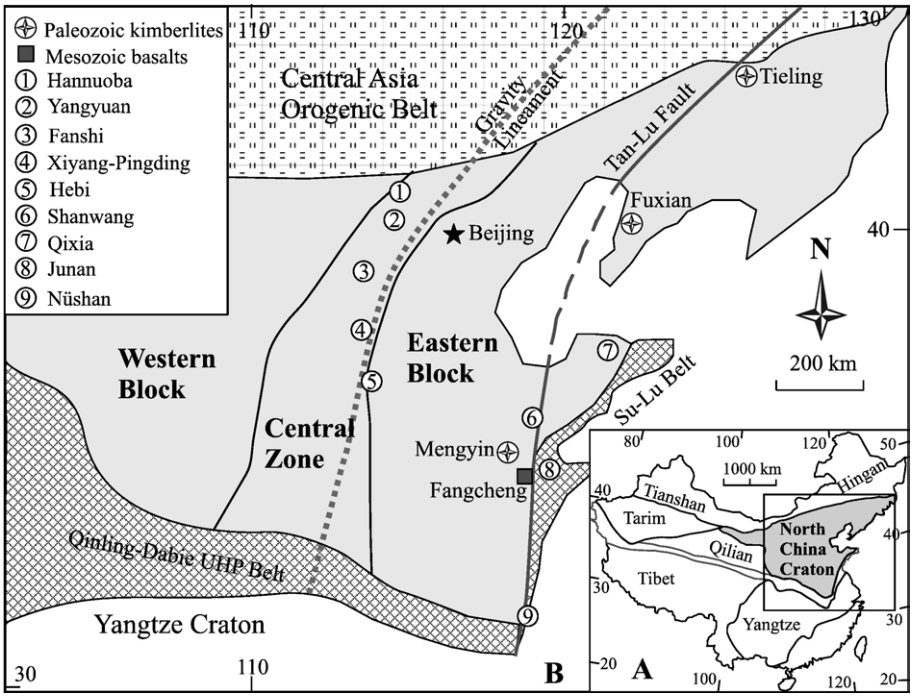

Fig. 1. Simplified geological map showing mantle xenolith localities mentioned in the text. The tectonic subdivisions of the NCC are from Zhao et al. (2002).

of thin (<80 km), hot and fertile lithosphere in the Cenozoic, which indicates the loss of more than 100 km of the ancient lithosphere beneath the eastern NCC during the Phanerozoic (Griffin et al., 1992; Menzies et al., 1993; Griffin et al., 1998; Fan et al., 2000). This remarkable evolution of the old sub-continental lithospheric mantle has attracted considerable attention in recent years (e.g. Menzies and Xu, 1998; Xu, 2001; Zheng et al., 2001; Gao et al., 2002a; Zhang et al., 2002; Zhang et al., 2003; Rudnick et al., 2004; Xu and Bodinier, 2004; Wu et al., 2005; Zhang, 2005; Rudnick et al., 2006; Ying et al., 2006; Tang et al., 2007).

Re–Os isotope data for peridotite xenoliths in Paleozoic kimberlites (Fuxian and Mengyin) and Tertiary alkali basalts (Hannuoba and Qixia, Fig. 1) reveal that the garnet and spinel peridotites from the Fuxian and Mengyin kimberlites have Archean T_{RD} ages (2500–3200 Ma) and the Hannuoba peridotites display a Re–Os isochron age of 1900 Ma, while the Qixia peridotites generally have young T_{RD} ages of 0–700 Ma, which indicates that the ancient refractory lithospheric keel beneath the eastern NCC was replaced by more fertile lithospheric mantle sometime after the Paleozoic (Gao et al., 2002a; Zhang et al., 2007b). Compositions of peridotite xenoliths from Hannuoba, the Central Zone of the NCC, reflect variable degrees (0–25%) of melt extraction from a primitive mantle source, and they are different from typical cratonic lithosphere (Rudnick et al., 2004). Two types of spinel-facies xenoliths, high-Mg# (≥92) and low-Mg# (<91) peridotites based on Fo in olivines, have been observed in the Cenozoic Hebi basalts (Zheng et al., 2001) and late Cretaceous Junan basaltic breccias (Ying et al., 2006) (Fig. 1). The high-Mg# peridotites were interpreted as relics of old lithospheric mantle (Zheng et al., 2001; Ying et al., 2006), while the low-Mg# peridotites are fertile in major elements, similar to the peridotite xenoliths from the Cenozoic Shanwang basalts (Zheng et al., 1998) (Fig. 1). Therefore, they were considered to represent newly accreted lithospheric mantle (Zheng et al., 1998, 2001; Ying et al., 2006). These observations, combined with the relatively low Fo in olivine xenocrysts in the Mesozoic Fangcheng basalts (Zhang, 2005), which are considered to be the products of peridotite–melt reaction that can transform high-Fo peridotite to low-Fo one, suggest that the NCC experienced significant modification after its formation.

The Daxing'anling–Taihangshan gravity lineament (Fig. 1) is an important geologic zone within the NCC, roughly overlapping the Central Zone of the NCC, and separates two topographically, tectonically and seismically different regions: the Western and the Eastern Blocks (Zhao et al., 2001; Xu 2007). Based on the methodology of different geochemical and isotopic

signatures between the lithospheric mantle and asthenosphere, Xu et al. (2004) compared the geochemistry of Cenozoic basalts and their xenoliths from the Western and Eastern Blocks and concluded that progressive lithospheric thinning occurred in the Western Block during the Cenozoic, but an opposite process, i.e. lithospheric thickening in the Eastern Block. The contrasting lithospheric evolution yields that the lithospheric mantle beneath the Eastern Block is stratified with old lithosphere and the underlying newly accreted one (Ying et al., 2006), whereas the lithospheric mantle beneath the Western Block may consist mainly of old lithospheric relicts after thermo-mechanical erosion (Xu et al., 2004; Xu, 2007), i.e. coupled thermo-mechanical and chemical erosion within the lithosphere–asthenosphere interface, which is considered as an important mechanism for thinning of the lithosphere (Xu 2001). It is known that the thinning of Archean lithosphere occurred primarily beneath the Eastern Block and previous interpretations of this event are mainly based on this region, whereas the architecture of the lithospheric mantle beneath the Central Zone of the NCC remains unclear.

In this paper, we report petrology, mineralogy, and trace-element and Sr–Nd isotopic data of clinopyroxenes (cpx) for spinel peridotite xenoliths from the Cenozoic Fanshi basalts in the Central Zone (Fig. 1). The nature of the subcontinental lithospheric mantle represented by these xenoliths and mantle processes involved in their origin will be discussed, with an attempt to understand the evolution of lithospheric mantle.

2. Geologic setting

The North China Craton is bounded to the north by the Central Asia Orogenic belt and to the south by the Qinling–Dabie–Sulu ultra-high pressure metamorphic belt (Fig. 1). It is one of the oldest continental nuclei in the world (Liu et al., 1992; Zheng et al., 2004) and is composed of two Archean nuclei of the Eastern and Western Blocks, which are separated by the Central Zone (Zhao et al., 2001, 2002) (Fig. 1). The Eastern Block has thin crust (<35 km), weakly negative to positive Bouguer gravity anomalies and high heat flow. Thus, the lithosphere is inferred to be less than 80–100 km thick under this block (Ma, 1989). In contrast, the Western Block has thick crust (>40 km), strong negative Bouguer gravity anomalies and low heat flow, reflecting a lithosphere of more than 100 km thickness (Ma, 1989). The basement of the NCC is composed of Archean to Paleoproterozoic tonalitic–trondhjemitic–granodiotitic gneisses and granitoids, interleaved with abundant sedimentary and volcanic rocks (Zhao et al., 2001). The Archean rocks of the Central Zone underwent compressional deformation and peak high-pressure metamorphism and were significantly reworked during the Paleoproterozoic (Zhao et al., 2001; Wang et al., 2003; Rudnick et al., 2006). In particular, it was considered that the NCC underwent ~1.8 Ga subduction/collision between the Eastern and Western Blocks, which formed the central orogen and resulted in the final amalgamation of the NCC (Zhao et al., 2001, 2002; Wang et al., 2003).

From its formation to the Mesozoic, the NCC remained quiescent with respect to magmatic and tectonic events, except for the eruption of kimberlites in the middle Ordovician (Lu et al., 1988) (Fig. 1). Since the Late Mesozoic this craton has experienced widespread tectono-thermal reactivation, as evidenced by emplacement of voluminous Late Mesozoic granites, mafic intrusions and volcanic rocks (Yang et al., 2003; Zhang et al., 2004), extensive Cenozoic volcanism of basalts carrying abundant mantle xenoliths (Zhou and Armstrong, 1982), and in particular, large-scale lithospheric thinning. This significant event is also reflected in a change in compositions of mantle xenoliths carried in Ordovician kimberlites versus Tertiary and Quaternary alkali basalts, from highly refractory to fertile in major elements (Menzies et al., 1993; Griffin et al., 1998; Fan et al., 2000).

3. Fanshi basalts and xenolith petrography

The Fanshi basaltic field lies to the south of Hannuoba basalts (Fig. 1). It covers an area of ~550 km^2, with a maximum thickness of 800 m. The Fanshi basalts erupted at 26–24 Ma; they are mainly alkaline and have OIB-like characteristics in their trace-element and isotopic compositions, indicating an asthenospheric source (see Figs. 7 and 8 in Tang et al., 2006). However, their large variations in elemental (Ba/Nb=6–22, La/Nb=0.5–1.0, Nb/U=29–50, Ce/Pb=15–30) and isotopic ratios ($^{87}Sr/^{86}Sr$=0.7038–0.7045, $^{143}Nd/^{144}Nd$=0.5124–0.5129) suggest the existence of some contributions of old lithospheric mantle to the basaltic magma. Therefore, the Fanshi basalts could result from the low degree partial melting of asthenosphere and the interaction of asthenosphere-derived magma with old lithospheric mantle in an extensional regime (Tang et al., 2006). The Fanshi basalts carry abundant spinel-facies peridotite and minor pyroxenite xenoliths. Here, attention is focused on the peridotite xenoliths.

Fanshi peridotite xenoliths are angular or rounded. 19 representative samples studied in this paper range from 5 to 7 cm across. They are mainly lherzolites (cpx>5%) with minor harzburgites (cpx<5%). Garnet, plagioclase

and water-bearing phases, such as mica and amphibole, have not been observed in these xenoliths.

The Fanshi harzburgites are coarse to medium-grained and have typical granular and porphyroblastic texture (Fig. 2A). They are relatively high in modal orthopyroxene content (opx 26–34%) and low in cpx (2–3%; Table 1), similar to those from the Hebi, China and the Kaapvaal craton, South Africa (Fig. 3). Mineral phases in the harzburgites are homogeneous through the multiple analyses of inter- or intra-grains and show no exsolution lamellae. Large olivines are kink-banded and show irregular grain boundaries (Fig. 2A).

The lherzolites are mainly medium to fine-grained with some coarse-grained varieties. Most have equilibrated textures, but a few show a corona texture and curved grain boundaries. Cpx exsolution lamellae are observed occasionally in opx (Fig. 2B). Spinels occur as interstitial phases at grain boundaries of other minerals. Patches and small cracks of siliceous and alumina-rich glasses with daughter crystals of olivine, spinel and cpx are present along the boundary of mineral grains (Fig. 2C). Most mineral phases in the lherzolites are homogeneous except for a few with reaction rims (Fig. 2D). The lherzolites have cpx modes mostly higher than 10% (Table 1), similar to those from the widespread Cenozoic basalts in eastern China (Fig. 3B) (Fan et al., 2000).

4. Analytical methods

Representative samples were selected after thin section observation and crushed to <30 mesh, and then cpx separates were carefully handpicked under a binocular microscope. The cpx grains were cleaned in an ultrasonic bath with Milli-Q water and then leached with purified HCl before isotopic analysis.

Mineral modes in the peridotites (Table 1) were estimated by point counting of thin sections. Major element compositions of minerals (Table 2) were determined with a Cameca SX50 electron microprobe at the Institute of Geology and Geophysics (IGG), Chinese Academy of Sciences, which were performed with a beam of 15 keV and 10 nA focused to a spot of ~2 μm in diameter. Natural mineral standards were used for calibration and a PAP correction procedure was applied to the data (Pouchou and Pichoir, 1991). The precision of the analyses is better than 5% for major components.

Trace-element analyses of cpx were carried out using a laser-ablation microprobe coupled to an ICP-MS at the Northwest University. The laser-ablation system is a GeolLas 200M, equipped with a 193 nm ArF excimer laser and a homogenizing imaging optical system. The ICP-MS is an Elan 6100-DRC. NIST 610 and CaO

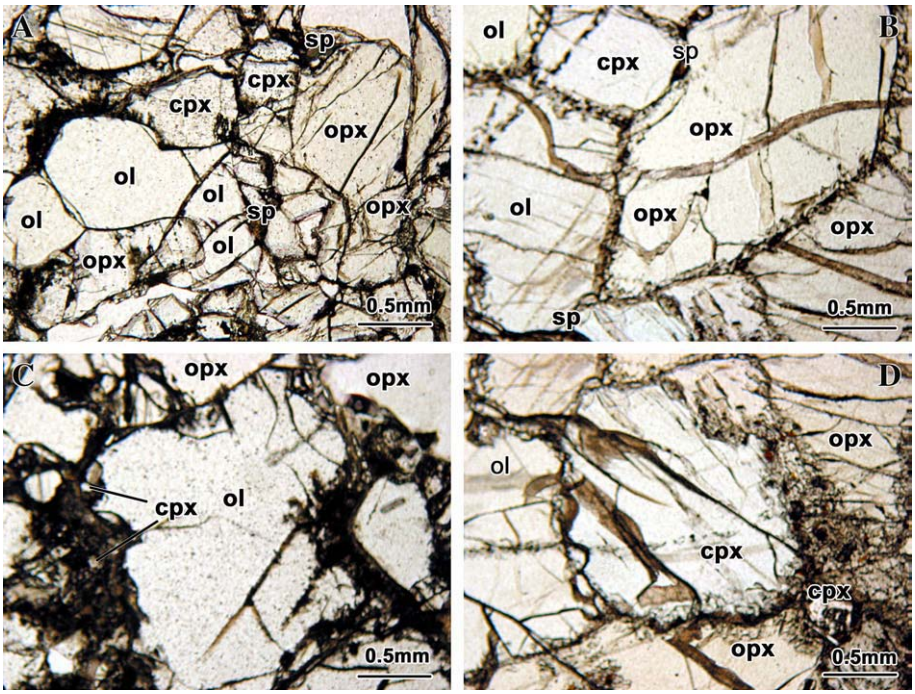

Fig. 2. Photomicrographs of representative textures of the spinel peridotites (plane polarized light). (A) FS12 shows granular and porphyroblastic texture with triple junctions. (B) FS14-1 shows curved boundaries of grains and exsolution lamellae in opx. (C) FS11-3 has patches with siliceous and alumina-rich glasses, containing many daughter crystals of olivine, spinel and cpx. (D) FS14-2 is foliated and shows reaction rims around pyroxenes.

Table 1
Mineral modes (vol.%) of Fanshi peridotites

Sample	Ol	Opx	Cpx	Sp
Sp-lherzolite				
FS3	76	15	7	2
FS4	70	17	8	5
FS4-2	70	16	10	4
FS5	62	24	13	1
FS10	61	20	15	4
FS11-3	69	20	10	1
FS13-2	66	21	12	1
FS14-1	65	22	12	1
FS14-2	67	23	9	1
FS15-1	63	24	11	2
FS15-2	68	14	16	2
FS21	63	21	15	1
FS22	61	20	18	1
FS29-2	59	18	20	3
FS32	63	13	21	3
Sp-harzburgite				
FS11-2	68	26	3	3
FS12	61	34	3	2
FS16	67	30	2	1
FS26	65	32	2	1

Ol = olivine; opx = orthopyroxene; cpx = clinopyroxene; sp = spinel.

contents were used as external and internal standards, respectively. Data were reduced using the Glitter software. Trace-element abundances given in Table 3 are averages of at least three analyses for each sample. Analytical details and results for NIST SRM (610, 612, 614) standards have been reported in Gao et al. (2002b).

Sr and Nd isotopic compositions were measured using a Finnigan MAT-262 thermal ionization mass spectrometer at the IGG. After leaching with sub-boiling distilled 6 M HCl for 30 min, the cpx separates were rinsed with Milli-Q water and dried. Then, they were ground by hand with an agate mortar to 200 mesh. The powders were weighed (~150 mg) and dissolved in distilled $HF+HNO_3$ in Teflon beakers at 150 °C for 7 days. The solutions were dried and then dissolved in dilute HCl before loading on columns filled with AG50W-X8 resin for separation and purification of Rb, Sr and REE, using 2.5 N and 4 N HCl as eluants. The separation of Sm and Nd from the bulk REE was performed on HDEHP columns, using HCl as eluant. The mass fractionation corrections for Sr and Nd isotope ratios were based on $^{86}Sr/^{88}Sr=0.1194$ and $^{146}Nd/^{144}Nd=0.7219$. Repeat analyses yielded $^{87}Sr/^{86}Sr$ of 0.710253 ± 0.000010 for the NBS-987 standard and $^{143}Nd/^{144}Nd$ of 0.511862 ± 0.000011 for the La Jolla standard.

5. Results

5.1. Major element data

The minerals in the peridotites are homogeneous, except for FS14-2 based on determination of individual

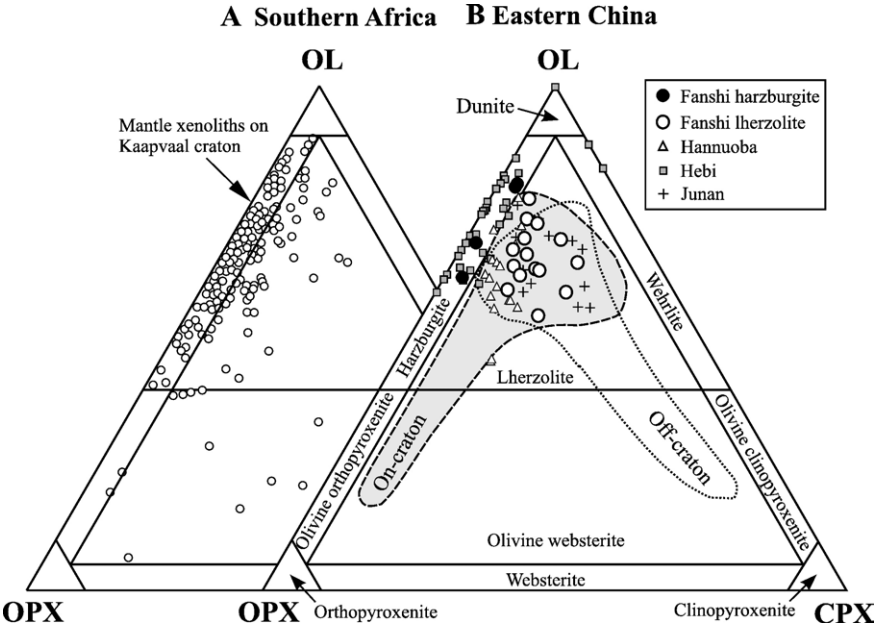

Fig. 3. Petrologic classification of the peridotites. Data sources: Hannuoba (Song and Frey, 1989; Fan et al., 2000; Rudnick et al., 2004); Hebi (Fan et al., 2000; Zheng et al., 2001); Junan (Ying et al., 2006); on- and off-craton peridotites from the Cenozoic basalts in eastern China, and old peridotites from the Kaapvaal craton, South Africa (Fan et al., 2000, and references therein).

Table 2
Representative electron microprobe analyses (wt.%) of minerals from the Fanshi peridotites

Sample	FS3			FS4				FS4-2				FS5				FS11-3			
Rock	Sp-lherzolite			Sp-lherzolite				Sp-lherzolite				Sp-lherzolite				Sp-lherzolite			
Mineral	Ol	Cpx	Opx	Ol	Cpx	Opx	Sp	Ol	Cpx	Opx	Sp	Ol	Cpx	Opx	Sp	Ol	Cpx	Opx	Sp
Point	5	5	4	5	7	5	4	5	5	6	4	6	5	5	4	7	5	6	4
SiO_2	41.01	52.65	54.79	40.49	53.98	56.14		40.89	53.69	56.98		41.24	52.64	55.22		40.81	52.10	54.98	
TiO_2		0.37	0.11		0.25	0.07	0.08		0.24	0.04	0.12		0.45	0.04	0.10		0.11	0.15	0.06
Al_2O_3		4.47	3.24		5.03	3.88	51.22		4.82	3.87	52.16		5.74	3.67	53.63		4.57	3.99	51.58
Cr_2O_3		0.83	0.48		0.74	0.45	16.37		0.78	0.37	15.64		0.94	0.28	13.06		0.70	0.29	16.63
FeO	9.23	2.35	6.06	9.75	2.29	5.49	10.81	9.57	2.25	5.35	9.63	10.00	2.58	6.28	11.44	10.04	2.95	6.28	10.68
MnO	0.14	0.04	0.15	0.13	0.08	0.10	0.17	0.13	0.02	0.13	0.08	0.14	0.05	0.10	0.12	0.11	0.07	0.21	0.13
MgO	49.77	15.29	33.44	49.40	16.10	33.33	20.28	49.33	16.02	33.47	20.59	48.51	15.51	33.02	20.21	49.33	18.02	33.65	19.89
CaO	0.08	21.53	0.69	0.03	20.12	0.66		0.07	20.08	0.70		0.06	19.28	0.60		0.03	21.41	0.54	
Na_2O		1.80	0.04		1.39	0.15			1.25	0.08			1.39	0.08			1.28	0.09	
NiO	0.38	0.02	0.05	0.42	0.08	0.00	0.28	0.47	0.11	0.06	0.34	0.36	0.13	0.00	0.29	0.31	0.12	0.09	0.30
Total	100.6	99.5	99.1	100.2	100.1	100.3	99.2	100.5	99.3	101.0	98.6	100.3	98.7	99.3	98.8	100.6	100.3	100.3	99.3
Mg#	90.7	92.1	90.9	90.1	92.7	91.6	78.7	90.3	92.8	91.8	79.4	89.7	91.5	90.4	76.1	89.8	91.2	90.6	74.3
Cr#		11.1	9.1		8.9	7.2	17.7		9.7	6.0	16.8		9.9	4.9	14.0		9.3	4.7	17.8

Sample	FS10			FS13-2				FS14-1				FS14-2							
Rock	Sp-lherzolite			Sp-lherzolite				Sp-lherzolite				Sp-lherzolite							
Mineral	Ol	Cpx	Opx	Ol	Cpx	Opx	Sp	Ol	Cpx	Opx	Sp	Ol-c	Ol-m	Ol-r	Cpx-c	Cpx-r	Cpx-c	Opx-r	Sp
Point	4	6	6	4	4	5	5	4	5	5	6	6	4	4	6	5	6	4	4
SiO_2	39.52	50.21	55.09	40.87	51.82	55.53		40.58	51.63	55.14		40.05	40.33	40.19	52.88	52.08	54.01	54.98	
TiO_2		0.79	0.25		0.60	0.09	0.15		0.52	0.17	0.15				0.24	0.28	0.02	0.05	0.13
Al_2O_3		5.72	4.77		6.07	4.10	57.00		6.95	4.32	59.19				4.73	5.44	4.51	4.22	52.97
Cr_2O_3		0.37	0.13		0.78	0.34	11.79		0.63	0.26	9.08				0.62	0.70	0.43	0.37	13.79
FeO	13.45	3.53	8.20	9.97	2.64	6.15	10.70	10.64	2.94	6.56	10.94	9.93	10.03	12.01	2.74	3.00	6.18	6.29	10.90
MnO	0.16	0.08	0.17	0.12	0.10	0.16	0.11	0.17	0.12	0.13	0.10	0.11	0.17	0.15	0.05	0.07	0.08	0.10	0.17
MgO	45.62	15.32	30.63	49.71	15.61	33.85	20.43	49.03	15.27	33.25	20.84	49.58	49.54	47.93	16.86	16.71	34.02	33.30	21.63
CaO	0.11	21.65	0.78	0.08	20.77	0.58		0.06	19.95	0.67		0.09	0.07	0.18	21.49	20.94	0.71	0.69	
Na_2O		0.77	0.11		1.57	0.09			1.86	0.10					1.00	1.06	0.05	0.06	
NiO	0.50	0.01	0.2	0.39	0.04	0.03	0.36	0.38	0.07	0.05	0.47	0.35	0.38	0.32	0.04	0.05	0.03	0.03	0.25
Total	99.4	98.8	100.3	101.1	100.0	100.9	100.6	100.9	99.9	100.6	100.8	100.1	100.5	100.8	100.7	100.3	100.0	100.1	99.8
Mg#	85.9	88.6	87.1	90.0	91.4	90.8	77.3	89.2	90.3	90.1	77.4	90.0	89.9	87.8	91.7	90.9	90.8	90.5	63.9
Cr#		4.2	1.8		8.0	5.2	12.2		5.7	3.9	9.3				8.1	7.9	6.0	5.6	14.9

Sample	FS15-1				FS15-2				FS21				FS22				FS29-2			
Rock	Sp-lherzolite				Sp-lherzolite				Sp-lherzolite				Sp-lherzolite				Sp-lherzolite			
Mineral	Ol	Cpx	Opx	Sp	Ol	Cpx	Opx	Sp	Ol	Cpx	Opx	Sp	Ol	Cpx	Opx	Sp	Ol	Cpx	Opx	Sp
Point	5	5	6	4	5	7	6	4	6	6	5	4	6	6	6	4	5	4	5	4
SiO_2	40.49	53.09	55.63		40.21	52.66	55.48		40.41	51.67	54.77		40.47	52.73	54.95		40.81	52.42	54.62	
TiO_2		0.40	0.12	0.14		0.18	0.16	0.13		0.60	0.12	0.17		0.55	0.10	0.09		0.28	0.09	0.06
Al_2O_3		5.18	3.42	50.00		6.81	4.16	57.45		4.80	4.58	58.36		6.81	4.44	58.27		4.49	4.32	56.03
Cr_2O_3		1.01	0.34	16.78		0.70	0.35	8.87		0.85	0.34	9.28		0.54	0.27	9.68		0.59	0.31	10.06
FeO	9.95	2.47	5.82	11.29	10.39	2.93	6.35	10.83	10.55	2.77	6.65	10.64	10.89	3.06	6.81	10.76	10.75	2.85	6.87	12.12
MnO	0.15	0.10	0.15	0.11	0.13	0.10	0.12	0.09	0.17	0.10	0.14	0.12	0.15	0.10	0.17	0.09	0.12	0.12	0.10	0.17
MgO	49.37	15.67	33.36	19.89	48.56	15.47	32.96	20.77	48.91	16.97	32.81	20.69	48.90	15.32	33.18	20.99	48.30	16.25	32.79	19.89
CaO	0.03	20.55	0.64		0.05	19.75	0.70		0.09	21.32	0.63		0.09	19.94	0.44		0.08	22.23	0.68	
Na_2O		1.39	0.09			1.75	0.12			1.16	0.10			1.80	0.12			1.41	0.09	
NiO	0.36	0.06	0.17	0.23	0.39	0.14	0.00	0.41	0.40	0.09	0.00	0.38	0.37	0.08	0.00	0.39	0.44	0.02	0.00	0.39
Total	100.4	99.9	99.7	98.4	99.7	100.5	100.4	98.5	100.5	100.3	100.1	99.6	100.9	100.3	100.5	100.3	100.5	100.7	99.9	98.7
Mg#	89.9	92.0	91.2	76.0	89.4	90.5	90.3	77.5	89.3	91.7	89.9	77.8	89.0	90.0	89.8	77.8	89.0	91.1	89.6	74.7
Cr#		11.6	6.3	18.4		6.5	5.4	9.4		10.6	4.7	9.6		5.1	3.9	10.0		8.1	4.5	10.8

Sample	FS32				FS11-2				FS12				FS16				FS26			
Rock	Sp-lherzolite				Sp-harzburgite				Sp-harzburgite				Sp-harzburgite				Sp-harzburgite			
Mineral	Ol	Cpx	Opx	Sp	Ol	Cpx	Opx	Sp	Ol	Cpx	Opx	Sp	Ol	Cpx	Opx	Sp	Ol	Cpx	Opx	Sp
Point	6	6	5	4	5	6	5	4	6	6	6	4	6	6	6	4	5	5	5	4
SiO_2	40.56	51.34	54.59		41.65	53.99	56.54		41.08	53.76	56.14		41.07	53.82	55.59		41.05	53.29	55.15	
TiO_2		0.36	0.09	0.13		0.25	0.01	0.11		0.22	0.02	0.10		0.28	0.11	0.08		0.18	0.03	0.05
Al_2O_3		4.95	4.36	56.44		4.98	3.18	52.53		5.18	3.07	51.79		4.39	3.14	44.44		6.07	3.35	44.79
Cr_2O_3		0.72	0.28	10.06		0.81	0.41	15.55		1.99	0.58	17.97		1.16	0.46	24.18		2.04	0.57	24.43
FeO	10.72	3.09	6.84	11.45	8.75	2.34	5.41	9.76	8.29	2.20	5.19	11.41	8.37	2.20	5.16	10.74	8.24	2.17	5.08	10.75
MnO	0.16	0.09	0.11	0.09	0.12	0.06	0.13	0.08	0.14	0.09	0.08	0.15	0.05	0.07	0.14	0.12	0.03	0.10	0.06	0.12
MgO	48.16	16.64	32.89	20.86	49.52	16.20	33.38	20.54	49.51	15.74	33.80	18.48	50.67	16.44	34.67	19.08	50.84	16.70	33.67	19.23
CaO	0.09	21.87	0.58		0.07	19.97	0.69		0.05	18.30	0.55		0.04	19.59	0.59		0.03	17.53	0.68	
Na_2O		1.40	0.08			1.24	0.08			1.08	0.14			0.85	0.04			1.03	0.19	
NiO	0.39	0.02	0.00	0.42	0.43	0.05	0.12	0.40	0.38	0.10	0.00	0.26	0.32	0.03	0.06	0.28	0.36	0.15	0.13	0.27
Total	100.1	100.5	99.8	99.5	100.5	99.9	99.9	99.0	99.5	98.7	99.6	100.2	100.5	98.8	100.0	98.9	100.5	99.3	98.9	99.8
Mg#	89.0	90.7	89.6	76.6	91.1	92.6	91.7	79.1	91.5	92.8	92.1	74.5	91.6	93.1	92.4	76.2	91.7	93.3	92.3	76.3
Cr#		8.9	4.1	10.7		9.8	7.9	16.6		20.5	11.3	18.9		15.1	9.0	26.7		18.4	10.2	26.8

Ol = olivine; opx = orthopyroxene; cpx = clinopyroxene; sp = spinel; c = core; m = mantle; r = rim; Mg# = 100×molar Mg/(Mg+Fe); Cr# = 100×molar Cr/(Cr+Al).

Table 3
Trace-element concentrations (ppm) in clinopyroxenes from the Fanshi xenoliths

Sample	*Sp-lherzolite*									
	FS3	FS4	FS4-2	FS5	FS10	FS11-3	FS13-2	FS14-1	FS14-2c	FS14-2r
Ba	6.80	1.44	1.33	1.78	4.04	1.32	1.12	2.63	0.66	0.45
Sr	264	178	133	170	333	201	204	463	253	356
Y	12.7	12.4	12.3	13.1	15.6	16.7	17.4	12.5	17.3	18.9
Zr	12.5	25.8	19.7	11.6	39.0	11.1	36.5	37.1	12.7	36.1
Hf	0.52	0.87	0.90	0.40	0.97	0.38	1.40	1.16	0.44	1.09
Nb	0.56	0.49	0.46	0.60	0.17	0.16	0.12	0.49	0.10	0.24
La	8.39	3.91	6.39	8.72	15.7	3.68	6.87	11.4	4.11	12.9
Ce	13.2	8.59	11.5	15.4	30.3	5.58	13.6	24.3	10.5	18.9
Pr	1.38	1.16	1.45	1.75	3.21	0.68	1.72	2.71	1.62	2.18
Nd	5.64	5.27	5.91	6.67	13.4	3.98	7.58	10.4	7.81	8.76
Sm	1.52	1.37	1.82	1.67	3.10	1.52	2.03	2.57	2.55	2.68
Eu	0.50	0.49	0.60	0.55	1.07	0.63	0.77	0.78	0.81	0.94
Gd	1.61	1.67	2.03	1.72	3.56	2.19	2.67	2.61	2.76	2.99
Tb	0.28	0.28	0.36	0.31	0.58	0.43	0.45	0.44	0.49	0.51
Dy	1.85	1.94	2.10	1.96	3.63	2.74	2.89	2.46	3.04	3.21
Ho	0.41	0.45	0.45	0.42	0.69	0.66	0.68	0.53	0.69	0.74
Er	1.17	1.27	1.27	1.18	1.85	1.77	2.02	1.40	1.90	2.02
Tm	0.17	0.19	0.19	0.18	0.27	0.28	0.29	0.20	0.29	0.30
Yb	1.18	1.19	1.26	1.26	1.82	1.86	1.87	1.30	1.96	2.02
Lu	0.18	0.18	0.18	0.19	0.28	0.26	0.29	0.19	0.29	0.30
Th	3.39	1.11	1.22	0.62	2.35	3.21	0.73	1.88	0.86	1.63
U	0.75	0.22	0.33	0.16	0.51	0.68	0.22	0.41	0.40	0.37
ΣREE	37	28	35	42	79	26	44	61	39	58
$(La/Yb)_n$	4.9	2.3	3.5	4.8	6.0	1.4	2.5	6.1	1.5	4.4

Sample	*Sp-lherzolite*									
	FS15-1	FS15-2	FS21	FS22	FS29-2	FS32	FS11-2	FS12	FS16	FS26
Ba	1.77	4.24	5.01	4.85	6.08	1.91	7.47	0.78	2.39	0.11
Sr	252	220	181	191	580	169	142	32	311	20
Y	19.4	15.0	22.7	14.7	16.0	22.4	9.69	9.46	11.2	8.58
Zr	24.2	22.9	20.1	30.5	23.3	24.2	11.8	6.98	40.6	6.67
Hf	1.05	0.96	0.87	0.87	0.68	0.82	0.54	0.35	1.15	0.23
Nb	0.20	0.18	1.15	0.81	0.91	0.22	1.31	0.23	0.33	0.15
La	9.61	8.71	5.11	4.93	16.2	2.76	8.23	0.55	14.8	0.27
Ce	19.8	17.1	13.5	10.1	48.2	4.93	15.9	1.98	26.0	1.13
Pr	2.65	2.05	2.06	1.19	7.21	0.86	1.92	0.38	2.97	0.23
Nd	11.8	8.20	9.36	5.27	27.7	4.58	8.46	2.28	12.4	1.52
Sm	2.93	2.39	2.84	1.68	5.55	2.02	1.75	0.92	2.41	0.68
Eu	0.96	0.81	0.96	0.66	1.48	0.77	0.57	0.38	0.74	0.29
Gd	2.98	2.52	3.07	2.26	3.48	2.99	1.88	1.38	2.28	1.14
Tb	0.52	0.46	0.56	0.46	0.53	0.55	0.33	0.27	0.38	0.21
Dy	3.59	2.83	3.97	2.88	2.96	3.89	2.02	1.74	2.35	1.39
Ho	0.77	0.64	0.88	0.60	0.62	0.83	0.43	0.38	0.49	0.31
Er	2.12	1.78	2.50	1.73	1.68	2.40	1.19	1.01	1.25	0.88
Tm	0.32	0.26	0.38	0.24	0.26	0.35	0.17	0.15	0.18	0.13
Yb	2.16	1.75	2.35	1.57	1.63	2.37	1.11	0.95	1.12	0.83
Lu	0.33	0.26	0.34	0.24	0.24	0.34	0.16	0.14	0.16	0.12
Th	1.11	1.50	1.98	1.62	1.91	1.57	1.69	0.33	1.17	0.03
U	0.27	0.43	0.61	0.39	0.51	0.24	0.68	0.06	0.26	0.02
ΣREE	61	50	48	34	102	30	44	13	68	9
$(La/Yb)_n$	3.1	3.4	1.5	2.2	6.9	0.8	5.1	0.4	9.1	0.2

The subscript n denotes the chondrite-normalized element ratio (Anders and Grevesse, 1989).

phases between core and rim. The average composition is reported in Table 2 and plotted in Figs. 4–6.

Olivines from the lherzolites are generally lower in Mg# (Fo<91) (Fig. 4A) and higher in MnO and CaO contents than those from the harzburgites (Fig. 5). They plot in the field for Cenozoic peridotites (Fig. 5) and Phanerozoic lherzolites (Fig. 6A). Opx from the lherzolites have higher Al_2O_3 contents than those from the harzburgites (Fig. 4B). Cpx grains are high in Al_2O_3 and Cr_2O_3 (~0.5–1.0 wt.%) and are Cr-diopside. The Cr# in spinels and cpx from the lherzolites are lower than those from the harzburgites (Figs. 4D and 6B). In general, the mineral compositions and mineral assemblage of Fanshi lherzolites and Hannuoba peridotites overlap significantly (Figs. 3 and 4). They are also similar to those in Hebi and Junan low-Mg# peridotites (Figs. 3–5) and Shanwang lherzolites (Fig. 6B), as well as those in off-craton spinel peridotites worldwide (Fig. 4) (Rudnick et al., 2004).

The Fanshi harzburgites are similar to the high-Mg# peridotites from Hebi, Junan and old cratonic peridotites around the world, as shown in high opx/cpx modes (Fig. 3) and their mineral compositions, which plot into the field for the high-Mg# peridotites (Figs. 4–6). Compared with the lherzolites, the harzburgites have lower Al_2O_3 contents in pyroxenes, but higher Cr# in cpx and spinels (Figs. 4 and 6B). The olivines from the harzburgites are relatively higher in Fo (>91; Fig. 4A), lower in CaO and MnO contents, similar to the mantle olivine xenocrysts from the Cenozoic Xiyang–Pingding basalts (Tang et al., 2004) and Mesozoic Fangcheng basalts (Zhang, 2005) (Fig. 5), which are interpreted as relics of old lithospheric mantle fragments. Moreover, these olivines plot within or approach the field for those from old cratonic peridotites (Figs. 5 and 6A). The compositions of the harzburgites are, therefore, distinct from those of lherzolites, but similar to those of old cratonic peridotites, indicating a relatively refractory character of old lithospheric mantle.

5.2. Trace-element concentrations of cpx

Cpx from the peridotites display an overall large variation in chondrite-normalized REE patterns from LREE-depleted to LREE-enriched profiles (Fig. 7). For the harzburgites, both LREE-depleted and enriched REE patterns of cpx are observed (Fig. 7A); cpx from the harzburgites have HREE abundance around 5×CI chondrite values. In contrast, HREE contents in cpx from the lherzolites display a larger range. For instance, those from cpx-poor lherzolites are around 5×CI chondrite values (Fig. 7E), while those from other lherzolites, with strongly LREE-enriched (Fig. 7E) or transitional REE profiles (Fig. 7C), are around 10 to 20×CI chondrite values, much higher than those from

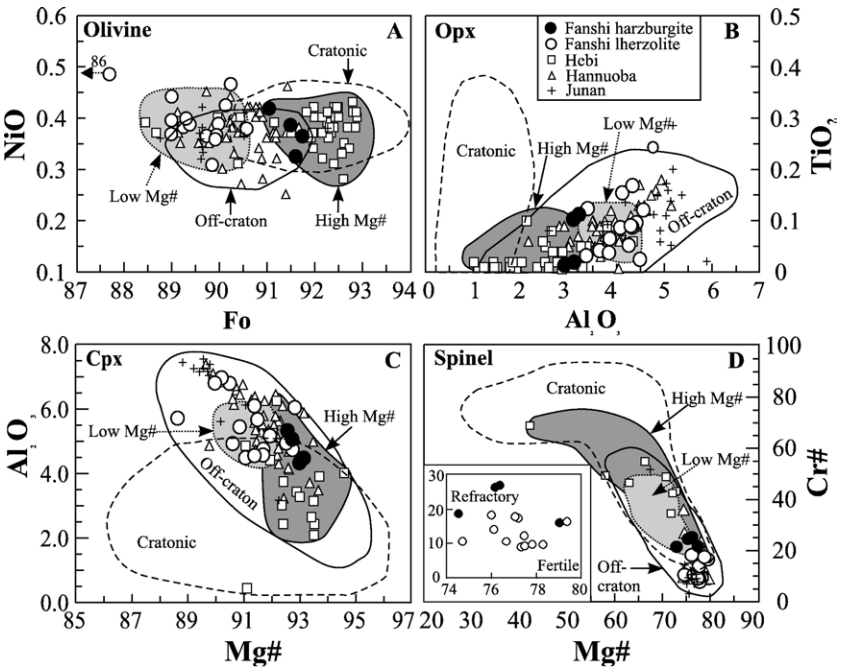

Fig. 4. Mineral compositions for the Fanshi peridotites compared with published data. Data sources: Hannuoba (Fan and Hooper, 1989; Song and Frey, 1989; Chen et al., 2001; Rudnick et al., 2004); Hebi (Fan and Hooper, 1989; Zheng et al., 2001); Junan (Ying et al., 2006); fields for worldwide off-craton spinel peridotites and cratonic (Kaapvaal, east Greenland, Siberia and Tanzania) peridotites (Rudnick et al., 2004).

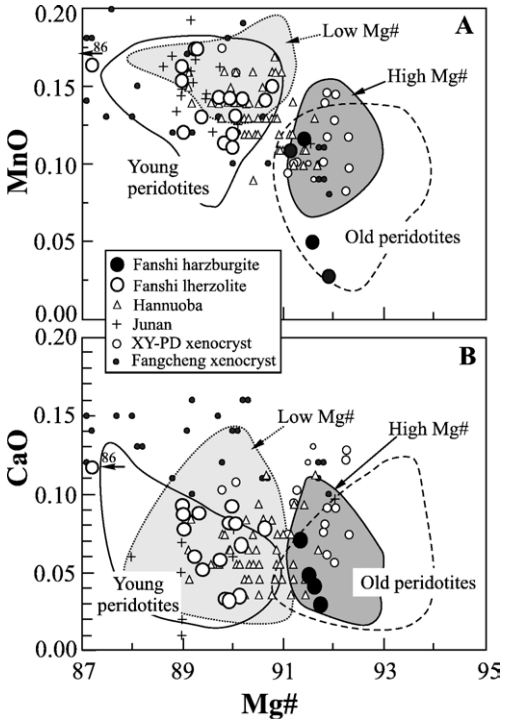

Fig. 5. Mg# vs. MnO (A) and CaO (B) of olivines from the Fanshi peridotites, compared with olivine xenocrysts in the Cenozoic Xiyang–Pingding (XY-PD) basalts (Tang et al., 2004) and Mesozoic Fangcheng basalts (Zhang, 2005), and young and old peridotites represent Paleozoic and Cenozoic peridotites, respectively (Fan et al., 2000; Zheng et al., 2001). Other data sources as the same in Fig. 4.

harzburgites. Lherzolites FS11-3 and FS32 display a spoon-shaped REE pattern (Fig. 7C), showing an enrichment of LREEs, which suggests that the effects of chromatographic metasomatism have modified the xenoliths, because chromatographic effect is that the trace-element composition of a melt may change dramatically along the percolation column, with more LREE than HREE and MREE near the percolation front due to the higher peridotite/melt partition coefficients of heavier REE than lighter REE (Navon and Stolper, 1987; Bodinier et al., 1990; Godard et al., 1995). Cpx from lherzolite FS14-2 has chemical zonation and its LREE is moderately enriched in the core (Fig. 7C), but strongly enriched in the rim (Fig. 7E). The FS29-2 has a convex-upward REE pattern of cpx.

In primitive mantle-normalized trace-element diagrams, cpx from the Fanshi samples generally display positive anomalies of Th and U and negative anomalies of high field strength elements (HFSE), for example Nb, Zr, Hf and Ti (Fig. 7). In addition, positive Sr anomalies and HFSE depletion in Cpx from the lherzolites are more remarkable than those of harzburgites (Fig. 7F). Their U, Th and Sr concentrations are elevated, possibly due to later enrichment processes by infiltration of small-volume melts (Bodinier et al., 2004).

5.3. Sr and Nd isotopes

Sr and Nd isotopic compositions of cpx from the Fanshi peridotites are given in Table 4. They range from bulk silicate earth-like Sr–Nd isotope ratios, to higher $^{87}Sr/^{86}Sr$ (0.7039–0.7060) and lower $^{143}Nd/^{144}Nd$ (0.5127–0.5118) than the Hannuoba peridotites (Fig. 8A). The large variation in the isotope ratios, from slightly depleted to enriched mantle (EM1), reflects an isotopic heterogeneity in the sub-continental lithospheric mantle, as observed in other on-craton peridotites worldwide (Fig. 8B).

The Sr–Nd isotopic compositions for the Fanshi lherzolites are relatively homogeneous and close to bulk silicate earth. Compared with the lherzolites, the harzburgites have more radiogenic Sr–Nd isotopic ratios, displaying a large range, an affinity to the on-craton peridotites

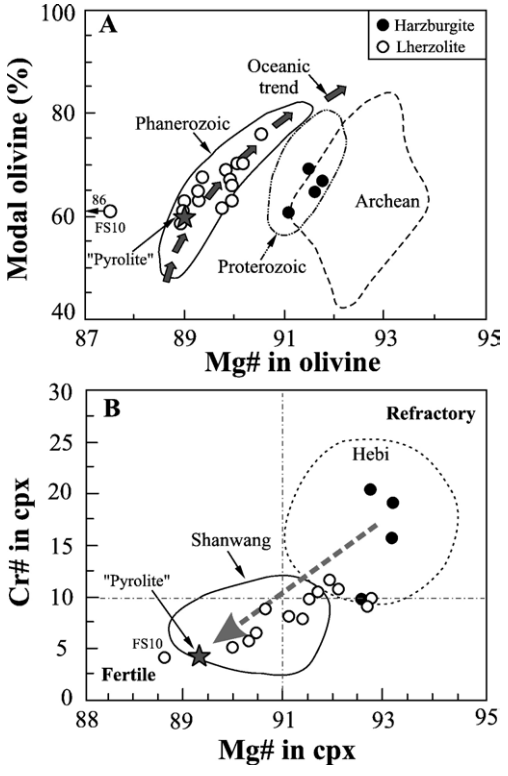

Fig. 6. (A) Mg# vs. modal (%) of olivines, (B) Mg# vs. Cr# in cpx from the Fanshi peridotites. Data sources: Hebi (Zheng et al., 2001); Shanwang (Zheng et al., 1998); "Pyrolite" (McDonough and Sun, 1995); oceanic peridotitic trend (Boyd, 1989); fields for Archean peridotites, Proterozoic and Phanerozoic lherzolites from Griffin et al. (1999).

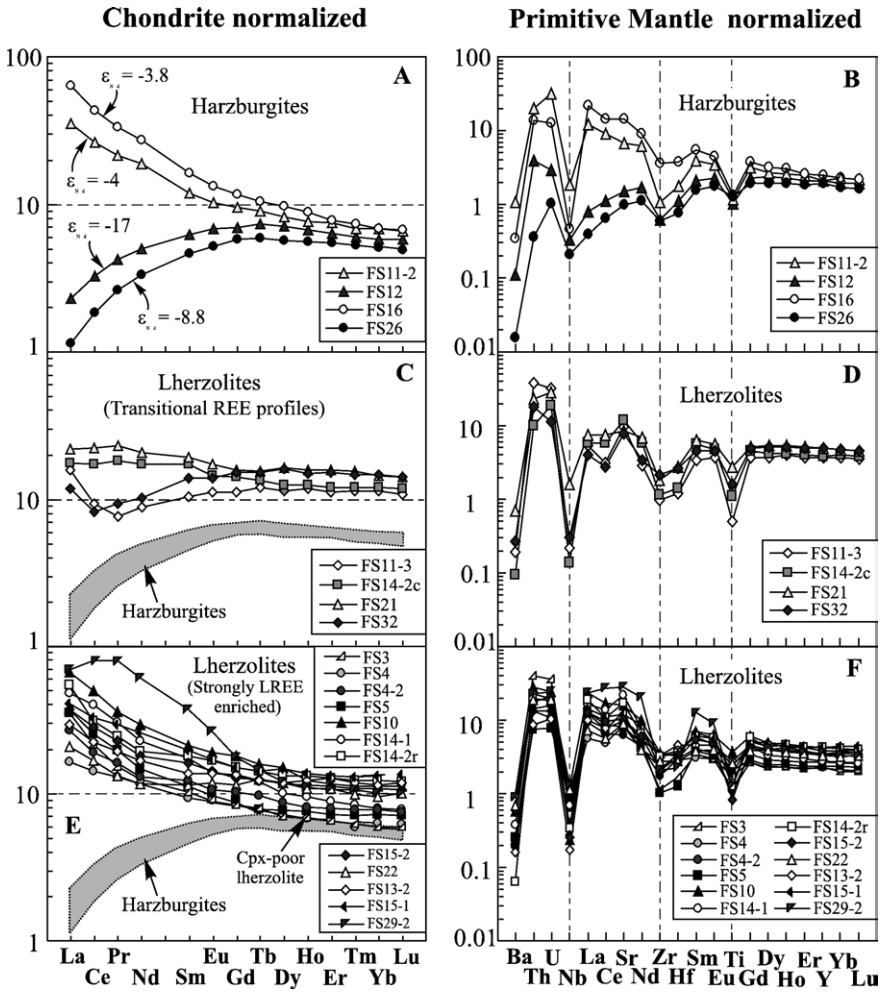

Fig. 7. Chondrite-normalized REE patterns and primitive mantle-normalized trace-element diagrams of cpx from the Fanshi peridotites. Chondrite and primitive mantle data are from Anders and Grevesse (1989) and Sun and McDonough (1989), respectively.

around the world (Fig. 8B). It is interesting that the sample FS12 displays a low $^{143}Nd/^{144}Nd$ ratio relative to its Sr isotope ratio and falls within the field for the Mesozoic lithospheric mantle as reflected by mafic rocks from the Central Zone (Fig. 8A). The harzburgites FS12 and FS26, with LREE-depleted patterns in cpx, have very low ε_{Nd} values (−17 and −8.8); while the FS11-2 and FS16 are LREE-enriched in cpx and have a much higher ε_{Nd} values (−4 and −3.8; Table 4).

6. Discussion

6.1. Mineral composition and origin

Major element data for Hannuoba peridotites reflect their origin as residues from partial melting of a primitive mantle source (Song and Frey, 1989; Rudnick et al., 2004). The mineral compositions in the Fanshi lherzolites are identical to those of Hannuoba xenoliths (Figs. 4 and 5), and could have originated from partial melting of a similar primitive mantle composition. Partial melting of a fertile peridotite will form a refractory lherzolite or harzburgite. Compared with the Fanshi lherzolites, relatively refractory mineral compositions of the harzburgites (high Mg# in olivines and pyroxenes, Cr# in spinels, and low Al_2O_3 and TiO_2 contents in pyroxenes; Fig. 4) indicate that they are residues from melting of a primitive mantle.

A typical feature of Archean mantle is the presence of highly refractory harzburgites and cpx-poor lherzolites (Boyd, 1989; Griffin et al., 1998). Generally, the peridotites become progressively less refractory from Archean through Proterozoic to Phanerozoic lithospheric mantle, and change from dominant harzburgites to predominant

Table 4
Sr and Nd isotopic data for clinopyroxene separates

Sample	Sm (ppm)	Nd (ppm)	$^{147}Sm/^{144}Nd$	$^{143}Nd/^{144}Nd$	2σ	ε_{Nd}	$^{87}Sr/^{86}Sr$	2σ
Lherzolite								
CP5	1.67	6.67	0.1514	0.512612	17	-0.5	0.704330	14
CP13-2	2.03	7.58	0.1619	0.512664	13	0.5	0.704381	11
CP14-1	2.57	10.4	0.1494	0.512677	14	0.8	0.703856	12
CP29-2	5.55	27.7	0.1211	0.512680	18	0.8	0.704012	15
SF20[a]	0.85	2.59	0.1984	0.512726	28	1.7	0.704103	7
Harzburgite								
CP11-2	1.75	8.46	0.1251	0.512435	15	−4.0	0.704800	10
CP12	0.92	2.28	0.2439	0.511767	18	−17	0.705951	15
CP16	2.41	12.4	0.1175	0.512445	19	−3.8	0.705366	17
CP26	0.68	1.52	0.2704	0.512185	15	−8.8	0.706039	13

[a]This sample is from Fan et al. (2000); $^{147}Sm/^{144}Nd$ were calculated from Sm and Nd concentrations in clinopyroxenes.

lherzolites (Griffin et al., 1998). Moreover, Archean subcontinental lithospheric mantle is believed to be the residue of high-degree melting of a primitive mantle (Griffin et al., 1999). As a result, there is a remarkable difference in mineral compositions between the Archean and Phanerozoic lithospheric mantle (Fig. 6A). The contrasting chemical compositions of peridotite xenoliths from Paleozoic kimberlites and Cenozoic basalts in eastern NCC (Griffin et al., 1992; Menzies et al., 1993; Griffin et al., 1998; Zheng et al., 1998, 2001; Rudnick et al., 2004; Zheng et al., 2006a) show a similar trend.

The above differences are also observed in the Fanshi peridotites. The harzburgites fall in or approach the fields for worldwide old cratonic peridotites in terms of Mg# in olivines and pyroxenes (Figs. 4 and 6), Cr_2O_3 in spinels, Al_2O_3 in pyroxenes (Fig. 4), and CaO and MnO in olivines (Fig. 5). These observations suggest that the harzburgites experienced high-degree melting and could be relics of old lithospheric mantle that was evidenced by the Re depletion model ages of >2.4 Ga for peridotite xenoliths from Cenozoic alkali basalts in the Fanshi and Yangyuan (Rudnick et al., 2006; Xu et al., 2007).

In contrast, nearly all the Fanshi lherzolites, similar to Hannuoba peridotites, fall within the fields for the off-craton peridotites and Phanerozoic lherzolites worldwide (Figs. 4–6). They are fertile in mineral compositions and show an oceanic trend (Fig. 6), and thus bear a resemblance to the newly accreted lithospheric mantle

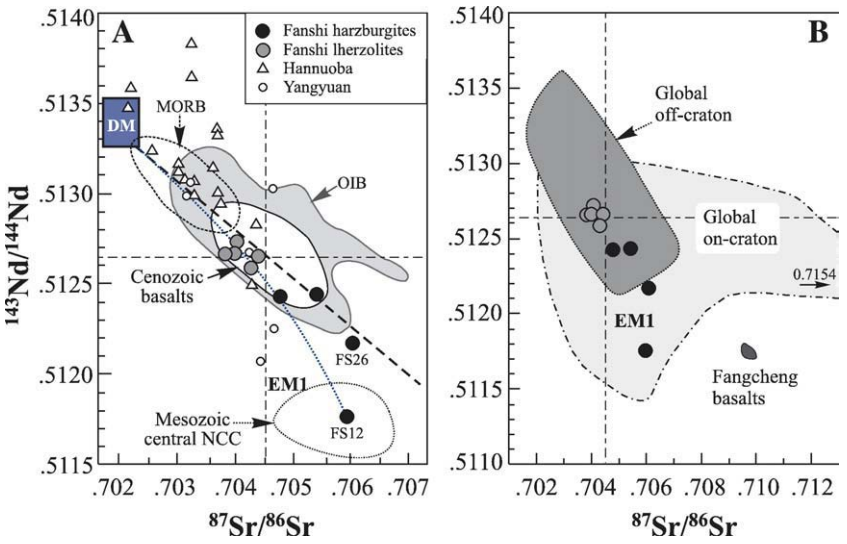

Fig. 8. (A) Sr and Nd isotope ratios in cpx from the Fanshi peridotites. Data sources: cpx from Hannuoba peridotites (Song and Frey, 1989; Tatsumoto et al., 1992; Rudnick et al., 2004), and Yangyuan peridotites (Ma and Xu, 2006); Mesozoic Fangcheng basalts (Zhang et al., 2002); Mesozoic lithospheric mantle beneath the central NCC (Zhang et al., 2004; Wang et al., 2006); Cenozoic Fanshi basalts (host basalts; Tang et al., 2006); DM, MORB, OIB and EM1 (Zindler and Hart, 1986). (B) Mantle peridotites from global on- and off-craton locations (Fan et al., 2000).

beneath eastern China (Fan et al., 2000). Here, the newly accreted lithospheric mantle is underlying old lithosphere with the thickening of lithosphere through an asthenospheric accretion due to thermal loss (Menzies and Xu, 1998). Nevertheless, Os isotopic data show a Paleoproterozoic age for the Fanshi peridotites (Rudnick et al., 2006), similar to the Re–Os correlation age of ~1.9 Ga for Hannuoba peridotites (Gao et al., 2002a). Namely, the Fanshi lherzolites are likely the fragments modified from the "old" lithosphere mantle. Since many studies have documented that old lithospheric mantle beneath the NCC had a refractory primary feature (Griffin et al., 1992; Menzies et al., 1993; Griffin et al., 1998; Zheng et al., 1998, 2001, 2006a). Now the question is what process has made the refractory mantle lithosphere fertile?

We suggest that recent asthenospheric melt–peridotite reaction is the cause, as proposed from the studies on mantle olivine xenocrysts and a highly-fertile lherzolite xenolith from the Mesozoic basalts (Zhang, 2005; Zhang et al., 2007a,b) and will be detailedly discussed in the following sections.

6.2. Trace-element patterns and mantle metasomatism

Trace-element patterns in cpx from these peridotites (Fig. 7) reflect multi-stage mantle processes. For the lherzolites, LREE enrichments in cpx mean that they have experienced later mantle metasomatism, while the spoon-shaped patterns (Fig. 7C) indicate a process of partial melting before chromatographic metasomatism of melt infiltration (Navon and Stolper, 1987). Meanwhile, the irregular REE profiles (Fig. 7C) also illustrate processes related to melt migration (Xu et al., 1998; Fan et al., 2000). Therefore, to interpret these data, we prefer a percolation-reaction model for the melt–rock reaction (Xu et al., 1998). The convex-upward REE pattern (Fig. 7E) confirms that a secondary melt infiltration process is involved subsequent to partial melting since this type of pattern is diagnostic of equilibrium with LREE-rich melts (Navon and Stolper, 1987; Bodinier et al., 1988; Xu and Bodinier, 2004).

LREE depletions in cpx from two harzburgites (Fig. 7A) show a partial melting process without significant later metasomatism, but their very low ε_{Nd} values suggest a long-term evolution of LREE enrichment before the partial melting process. As a result, this LREE enrichment of the harzburgites could happen much earlier than the later metasomatism of all these lherzolites and some harzburgites with LREE enrichments.

Since the original observation of Ti and Zr depletion relative to REE in cpx from many peridotites (Salters and Shimizu, 1988), opx was shown to be a significant repository for the HFSE budget (Rampone et al., 1991). Therefore, Ti depletion of the cpx (Fig. 7) may be an artifact of this process. Negative Nb and Zr anomalies are also a common feature of mantle diopside (Salters and Shimizu, 1988; Norman, 1998).

In summary, the metasomatic signatures in Fanshi cpx are evident in enrichments in LREE, Th, U (Fig. 7) and Sr (Fig. 9A). In addition, these cpx have low $(La/Yb)_n$ (0.2–9.1) and high Ti/Eu (500–8000) ratios, suggesting mainly silicate metasomatism (Fig. 9B).

6.3. Isotopic compositions and refertilization of ancient lithospheric mantle

It is notable that the Fanshi harzburgites display a large variation in their Sr–Nd isotope ratios (Fig. 8). Since the changes in Rb/Sr and Sm/Nd ratios associated with mantle metasomatism will, with time, lead to extreme isotopic heterogeneity, one can speculate that the cpx evolved from the mixing of a MORB-like lithospheric composition with several enriched components related to melt/fluid influx (Frey and Green, 1974). For instance, recycled or subducted fluids and melts may have considerable ranges in Sr/Nd ratios and isotopic compositions, and their influx may account for the apparent spread of the data (Fig. 8). One sample has an EM1-like isotopic signature of the Mesozoic lithospheric mantle beneath the same region (Fig. 8) that was

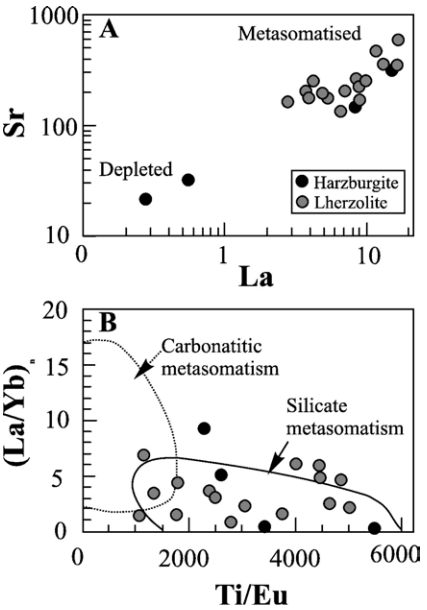

Fig. 9. Plots of La vs. Sr (A) and Ti/Eu vs. $(La/Yb)_n$ (B) in cpx from the Fanshi peridotites. Fields for "carbonatitic" and "silicate" metasomatism are after Coltorti et al. (1999).

considered to have been previously modified by silica-rich melts released from Paleoproterozoic subducted materials (Wang et al., 2006). The EM1-type mantle beneath the central NCC is also evidenced by the isotopic compositions of peridotite xenoliths in the Cenozoic basalts from Yangyuan (Fig. 8A) (Ma and Xu, 2006), and indicates a secular evolution of the sub-continental lithospheric mantle. Therefore, the isotopic features in Fanshi harzburgites may reflect ancient enrichment processes of the lithospheric mantle.

In contrast, the isotopic compositions for the Fanshi lherzolites are relatively homogeneous and close to bulk silicate earth (Fig. 8). The differences in Sr–Nd isotope ratios between the Fanshi lherzolites and harzburgites could have been produced by recent asthenospheric melt–peridotite reaction. As stated above, the harzburgites are believed to represent the relics of old lithospheric mantle. The reaction products (lherzolites) should be depleted in Sr–Nd isotopic compositions relative to the harzburgites owing to the depleted isotopic compositions of asthenospheric melt. However, the reaction may not cause the big change of Re–Os isotope system of mantle peridotites. This is because Os isotope systematics for cratonic peridotites appears to be dominantly influenced by the ancient differentiation events whereas Sr–Nd isotope systematics record later enrichment events (Pearson, 1999). Therefore, the Re–Os system is much more robust to peridotite–melt interaction (Pearson, 1999). For the Fanshi lherzolites, the emplacement of asthenospheric materials probably took place recently, as shown by the decoupling of high LREE/HREE ratios with relatively depleted isotopes. Recent peridotite–melt interaction can have produced only a small change in the Os isotope composition of mantle peridotites due to the low Os contents of percolating magmas (Lambert et al., 1989; Reisberg et al., 2005), and the insufficient time for a significant decay of ^{187}Re. In contrast, such interaction could result in a large change in Sr–Nd isotopic compositions of the peridotites (Lambert et al., 1989; Pearson, 1999; Pearson et al., 2003). This can also explain the observation that some peridotites are old in Os isotope ages but depleted in their Sr–Nd isotopic compositions.

The occurrence of pyroxenites among the Fanshi xenoliths, associated with the REE enrichments of cpx, corona textures and curved boundaries of grains in lherzolites (Fig. 2), indicates the existence of peridotite–melt reactions. In particular, the abundance of pyroxenites in Hannuoba xenoliths (Liu et al., 2005) further shows the pervasive reaction in the sub-continental lithospheric mantle. As a result, the peridotite–melt reaction might result in the different Sr–Nd isotopic compositions of cpx between lherzolites and harzburgites (Fig. 8).

Two of the Fanshi harzburgites with LREE enrichments in cpx (Fig. 7A) have less enriched isotopic ratios than another two harzburgites with LREE depletions in cpx, which are highly isotopic enriched (Fig. 8). This may argue that these two LREE-enriched harzburgites may also be affected by asthenospheric melt–peridotite reaction. This reaction led to the LREE enrichments and relatively isotopic depletion of a LREE-depleted and highly isotopic enriched harzburgite protolith. The conclusion has also been observed by the comparison of the hydrous and anhydrous mantle peridotite xenoliths from the central and western NCC (Zhao et al., 2007).

In summary, the petrology, mineralogy and elemental and isotopic geochemistry indicate that the lithospheric mantle section represented by the peridotite xenoliths has been refertilized by upward migration of asthenospheric melts, which leads to the transformation of ancient refractory lithospheric mantle into a fertile one.

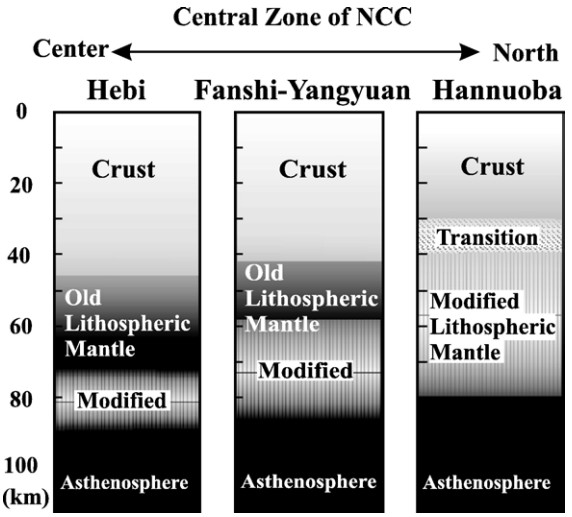

Fig. 10. Sketch map showing the lithospheric architecture beneath the Central Zone of the NCC. The lithospheric architecture is inferred from the mineral and Sr–Nd isotopic compositions of the peridotite xenoliths from these localities. The lithospheric mantle beneath the Hebi area mainly comprises relict of old lithospheric keel with minor lherzolites, which were modified by recent asthenospheric melt–peridotite reaction. In contrast, the lithospheric mantle beneath the Fanshi and Yangyuan are mainly modified lherzolites with minor harzburgites. The Hannuoba lithospheric mantle has been considerably modified by the asthenospheric melts as evidenced by the depleted isotopic compositions of peridotites. This melt–peridotite interaction and magma underplating also produced about 10 km crust–mantle transitional zone beneath the Hannuoba (Chen et al., 2001; Fan et al., 2005). However, the similar transitional zone has not been observed in the lithosphere beneath the interiors such as the Hebi and Fanshi–Yangyuan. In sum, the modification of lithospheric mantle by recent asthenospheric melt–peridotite reaction in the Central Zone is progressive and comprehensive from the interior to the northern margin of the NCC.

6.4. Lithospheric architecture beneath the Central Zone of NCC

Previous investigation of peridotite xenoliths from Hebi area, center of the Central Zone of the NCC (Fig. 1), reveals that the Hebi peridotites are mainly refractory harzburgites with minor less refractory to fertile lherzolites (Zheng et al., 2001, 2006a). In contrast, the Hannuoba peridotites in the northern margin of the NCC are mainly fertile lherzolites with minor harzburgites (Fig. 3) (Chen et al., 2001; Rudnick et al., 2004). The Sr–Nd isotopic compositions of the Hannuoba peridotites are very depleted (Fig. 8A), although they have old Re–Os isochron age of 1900 Ma (Gao et al., 2002a,b), which indicates that these peridotites have suffered from considerable modification of asthenospheric melt–peridotite reaction. Compared with the Hannuoba peridotites, some peridotites from the Yangyuan and Fanshi are highly enriched in the Sr–Nd isotopic compositions (Fig. 8A), implying small degrees of modification of the lithospheric mantle beneath the two areas. The highest Fo values and very refractory mineral compositions of the Hebi peridotites among the xenoliths from the Central Zone of the NCC (Fig. 4) suggest that they have experienced the least degrees of modification by the asthenospheric melts, which is also supported by their very old T_{RD} ages of >2500 Ma (Zheng et al., 2006b). Therefore, we suggest that the refertilization of the lithospheric mantle through the old peridotite–asthenospheric melt interaction became more progressive and comprehensive from the interior (e.g., Hebi area) to the north margin of the NCC (e.g., Hannuoba area) (Fig. 10), and that the modification of the lithospheric mantle beneath the Fanshi and Yangyuan is in the middle of the Hebi and Hannuoba areas.

7. Conclusions

The data presented here allow us to draw the following conclusions:

(1) Fanshi peridotite xenoliths are mainly spinel-facies lherzolites with minor harzburgites. The harzburgites (Fo>91) are relatively refractory in mineral compositions and have radiogenic Sr–Nd isotopic ratios. They are the relics of old lithospheric mantle beneath the central NCC.
(2) Fanshi lherzolites (Fo<91) are fertile in mineral compositions and have bulk silicate earth-like Sr–Nd. These features are different from the mantle peridotites beneath typical Archean cratons around the world.
(3) The heterogeneity of the lithospheric mantle represented by the xenoliths from Fanshi resulted from the multiple stage modification of peridotite–melt reaction. The final reaction led to the refertilization of ancient lithospheric mantle by the influx of asthenospheric melts.
(4) The refertilization of the lithospheric mantle through the old peridotite–asthenospheric melt interaction became more progressive and comprehensive from the interior (e.g., the Hebi where the lithospheric mantle was less affected) to the margin (e.g., the Hannuoba where the lithospheric mantle was considerably modified), with the modification of the lithospheric mantle beneath the Fanshi and Yangyuan in the middle.

Acknowledgements

We would like to express our gratitude to Martin A. Menzies, Cin-Ty Lee, Heinz G. Stosch, two anonymous reviewers and editor Stephen Foley for their valuable comments and constructive reviews which help to improve the different versions of the manuscript. P. Xu, Y. G. Ma and Q. Mao are thanked for their assistance with electron microprobe analyses and F. K. Chen, Z. Y. Chu and C. F. Li with the Sr–Nd isotopic analyses at the State Key Laboratory of Lithospheric Evolution, Institute of Geology and Geophysics, Chinese Academy of Sciences. We also appreciate the assistance with ICP-MS analyses at the State Key Laboratory of Continental Dynamics, Northwest University, Xi'an. The authors gratefully acknowledge the financial support from the Natural Science Foundation of China (40534022), the Knowledge Innovation Program of the Chinese Academy of Sciences (KZCX2-YW-103) to H.F. Zhang and the Natural Science Foundation of China (40503004) to Y.J. Tang.

References

Anders, E., Grevesse, N., 1989. Abundances of the elements: meteoritic and solar. Geochim. Cosmochim. Acta 53, 197–214.
Bodinier, J.L., Dupuy, C., Dostal, J., 1988. Geochemistry and petrogenesis of Eastern Pyrenean peridotites. Geochim. Cosmochim. Acta 52, 2893–2907.
Bodinier, J.L., Vaseur, G., Vernieres, J., Dupuy, C., Fabries, J., 1990. Mechanisms of mantle metasomatism: geochemical evidence from the Lherz orogenic peridotite. J. Petrol. 31, 597–628.
Bodinier, J.L., Menzies, M.A., Shimizu, N., Frey, F.A., McPherson, E., 2004. Silicate, hydrous and carbonate metasomatism at Lherz, France: contemporaneous derivations of silicate melt–harzburgite reaction. J. Petrol. 45, 299–320.
Boyd, F.R., 1989. Compositional distinction between oceanic and cratonic lithosphere. Earth Planet. Sci. Lett. 96, 15–26.

Chen, S.H., O'Reilly, S.Y., Zhou, X.H., Griffin, W.L., Zhang, G.H., Sun, M., Feng, J.L., Zhang, M., 2001. Thermal and petrological structure of the lithosphere beneath Hannuoba, Sino-Korean Craton, China: evidence from xenoliths. Lithos 56, 267–301.

Coltorti, M., Bonadiman, C., Hinton, R.W., Siena, F., Upton, B.G.J., 1999. Carbonatite metasomatism of the oceanic upper mantle: evidence from clinopyroxenes and glasses in ultramafic xenoliths of Grande Comore, Indian Ocean. J. Petrol. 40, 133–165.

Downes, H., 2001. Formation and modification of the shallow subcontinental lithospheric mantle: a review of geochemical evidence from ultramafic xenolith suites and tectonically emplaced ultramafic massifs western and central Europe. J. Petrol. 42, 233–260.

Fan, Q.C., Hooper, P.R., 1989. The mineral chemistry of ultramafic xenoliths of Eastern China—implications for upper mantle composition and the paleogeotherms. J. Petrol. 30, 1117–1158.

Fan, W.M., Zhang, H.F., Baker, J., Jarvis, K.E., Mason, P.R.D., Menzies, M.A., 2000. On and off the north China craton: where is the Archaean keel? J. Petrol. 41, 933–950.

Fan, Q.C., Zhang, H.F., Sui, J.L., Zhai, M.G., Sun, Q., Li, N., 2005. Magma underplating and Hannuoba present crust–mantle transitional zone composition: xenolith petrological and geochemical evidence. Sci. in China (D) 48, 1089–1105.

Foley, S.F., Andronikov, A.V., Jacob, D.E., Melzer, S., 2006. Evidence from Antarctic mantle peridotite xenoliths for changes in mineralogy, geochemistry and geothermal gradients beneath a developing rift. Geochim. Cosmochim. Acta 70, 3096–3120.

Frey, F.A., Green, D.H., 1974. The mineralogy, geochemistry and origin of Iherzolite inclusions in Victorian basanites. Geochim. Cosmochim. Acta 38, 1023–1059.

Gao, S., Rudnick, R.L., Carlson, R.W., McDonough, W.F., Liu, Y.S., 2002a. Re–Os evidence for replacement of ancient mantle lithosphere beneath the North China craton. Earth Planet. Sci. Lett. 198, 307–322.

Gao, S., Liu, X.M., Yuan, H.L., Hattendorf, B., Gunther, D., Chen, L., Hu, S.H., 2002b. Determination of forty-two major and trace elements in USGS and NIST SRM glasses by laser ablation-inductively coupled plasma-mass spectrometry. Geostand. Newslett. 26, 181–195.

Godard, M., Bodinier, J.-L., Vasseur, G., 1995. Effects of mineralogical reactions on trace element redistributions in mantle rocks during percolation processes: a chromatographic approach. Earth Planet. Sci. Lett. 133, 449–461.

Griffin, W.L., O'Reilly, S.Y., Ryan, C.G., 1992. Composition and thermal structure of the lithosphere beneath South Africa, Siberia and China: proton microprobe studies. International Symposium on Cenozoic Volcanic Rocks and Deep-seated Xenoliths of China and its Environs, Beijing, p. 20.

Griffin, W.L., Zhang, A.D., O'Reilly, S.Y., Ryan, C.G., 1998. Phanerozoic evolution of the lithosphere beneath the Sino-Korean Craton. In: Flower, M.F.J., Chung, S.L., Lo, C.H., Lee, T.Y. (Eds.), Mantle Dynamics and Plate Interactions in East Asia. American Geophysical Union, Washington D.C., pp. 107–126.

Griffin, W.L., O'Reilly, S.Y., Ryan, C.G., 1999. The composition and origin of sub-continental lithospheric mantle. In: Fei, Y., Ber1tKa, C.M., Mysen, B.O. (Eds.), Mantle petrology: field observations and high-pressure experimentation: a tribute to Francis R. (Joe) Boyd. The Geochemical Society Special Publication, Houston, pp. 13–45.

Lambert, D.D., Morgan, J.W., Walker, R.J., Shirey, S.B., Carlson, R.W., Zientek, M.L., Koski, M.S., 1989. Rhenium–osmium and samarium–neodymium isotopic systematics of the Stillwater Complex. Science 244, 1169–1174.

Lu, F.X., Wang, Y., Chen, M.H., Zheng, J.P., 1988. Geochemical characteristics and emplacement ages of Mengyin kimberlite, Shandong provinces, China. Int. Geol. Rev. 40, 998–1006.

Liu, D.Y., Nutman, A.P., Compston, W., Wu, J.S., Shen, Q.H., 1992. Remnants of 3800 Ma crust in the Chinese part of the Sino-Korean craton. Geology 20, 339–342.

Liu, Y.S., Gao, S., Lee, C.-T.A., Hu, S.H., Liu, X.M., Yuan, H.L., 2005. Melt–peridotite interactions: links between garnet pyroxenite and high-Mg# signature of continental crust. Earth Planet. Sci. Lett. 234, 39–57.

Ma, X., 1989. Atlas of active faults in China. Seismologic Press, Beijing. 120 pp.

Ma, J.L., Xu, Y.G., 2006. Old EM1-type enriched mantle under the middle North China Craton as indicated by Sr and Nd isotopes of mantle xenoliths from Yangyuan, Hebei Province. Chin. Sci. Bullet. 51, 1343–1349.

McDonough, W.F., Sun, S.S., 1995. The composition of the earth. Chem. Geol. 120, 223–253.

Menzies, M.A., Xu, Y.G., 1998. Geodynamics of the North China Craton. In: Flower, M.F.J., Chung, S.L., Lo, C.H., Lee, T.Y. (Eds.), Mantle Dynamics and Plate Interactions in East Asia. American Geophysical Union, Washington D.C, pp. 155–165.

Menzies, M.A., Fan, W.M., Zhang, M., 1993. Palaeozoic and Cenozoic lithoprobes and the loss of > 120 km of Archaean lithosphere, Sino-Korean craton, China. In: Prichard, H.M., Alabaster, T., Harris, N.B.W., Neary, C.R. (Eds.), Magmatic Processes and Plate Tectonics. Geological Society of London, Special Publication, pp. 71–81.

Navon, O., Stolper, E., 1987. Geochemical consequence of melt percolation—the upper mantle as a chromatographic column. J. Petrol. 95, 285–307.

Norman, M.D., 1998. Melting and metasomatism in the continental lithosphere: laser ablation ICPMS analysis of minerals in spinel lherzolites from eastern Australia. Contrib. Mineral. Petrol. 130, 240–255.

O'Reilly, S.Y., Griffin, W.L., Poudjom, Y.H., Morgan, P., 2001. Are lithosphere forever? Tracking changes in subcontinental lithospheric mantle through time. GSA Today 11, 4–10.

Pearson, D.G., 1999. Evolution of cratonic lithospheric mantle: an isotopic perspective. In: Fei, Y., Berka, C.M., Mysen, B.O. (Eds.), Mantle Petrology: Field Observations and High-Pressure Experimentation: A Tribute to Francis R (Joe) Boyd. The Geochemical Society Special Publication, pp. 57–78.

Pearson, D.G., Canil, D., Shirey, S.B., 2003. Mantle sample included in volcanic rocks: xenoliths and diamonds. In: Carlson, R.W. (Ed.), The Mantle and Core. Treatise on Geochemistry. Elsevier-Pergamon, Oxford, pp. 171–275.

Pouchou, J.L., Pichoir, F., 1991. Quantitative analysis of homogeneous or stratified microvolumes applying the model "PAP". In: Heinrich, K.F.J., Newbury, D.E. (Eds.), Electron Probe Quantification. Plenum, New York, pp. 31–75.

Rampone, E., Botazzi, P., Ottolini, L., 1991. Complementary Ti and Zr anomalies in orthopyroxene and clinopyroxene from mantle peridotites. Nature 354, 518–520.

Reisberg, L., Zhi, X., Lorand, J.-P., Wagner, C., Peng, Z., Zimmermann, C., 2005. Re–Os and S systematics of spinel peridotite xenoliths from east central China: evidence for contrasting effects of melt percolation. Earth Planet. Sci. Lett. 239, 286–308.

Rudnick, R.L., Gao, S., Ling, W.L., Liu, Y.S., McDonough, W.F., 2004. Petrology and geochemistry of spinel peridotite xenoliths from Hannuoba and Qixia, North China Craton. Lithos 77, 609–637.

Rudnick, R.L., Gao, S., Yuan, H.L., Puchtel, I., Walker, R., 2006. Persistence of Paleoproterozoic Lithospheric Mantle in the Central

Zone of the North China Craton, International Conference on Continental Volcanism-IAVCEI, Guangzhou, China, p. 26.
Salters, V.J.M., Shimizu, N., 1988. World-wide occurrence of HFSE-depleted mantle. Geochim. Cosmochim. Acta 52, 2177–2182.
Song, Y., Frey, F.A., 1989. Geochemistry of peridotite xenoliths in basalt from Hannuoba, eastern China: implications for subcontinental mantle heterogeneity. Geochim. Cosmochim. Acta 53, 97–113.
Sun, S.S., McDonough, W.F., 1989. Chemical and isotopic systematic of oceanic basalt: implication for mantle composition and processes. In: Saunders, A.D., Norry, M.J. (Eds.), Magmatism in the oceanic basins. Geological Society of London, Special Publication, pp. 313–346.
Tang, Y.J., Zhang, H.F., Ying, J.F., 2004. High-Mg olivine xenocrysts entrained in Cenozoic basalts in central Taihang Mountains: relicts of old lithospheric mantle. Acta Petrologica Sinica 20, 1243–1252.
Tang, Y.J., Zhang, H.F., Ying, J.F., 2006. Asthenosphere–lithospheric mantle interaction in an extensional regime: implication from the geochemistry of Cenozoic basalts from Taihang Mountains, North China Craton. Chem. Geol. 233, 309–327.
Tang, Y.J., Zhang, H.F., Nakamura, E., Moriguti, T., Kobayashi, K., Ying, J.F., 2007. Lithium isotopic systematics of peridotite xenoliths from Hannuoba, North China Craton: implications for melt-rock interaction in the considerably thinned lithospheric mantle. Geochim. Cosmochim. Acta 71, 4327–4341.
Tatsumoto, M., Basu, A.R., Huang, W.K., Wang, J.W., Xie, G.H., 1992. Sr, Nd, and Pb isotopes of ultramafic xenoliths in volcanic rocks of eastern China: enriched components EMI and EMII in subcontinental lithosphere. Earth Planet. Sci. Lett. 113, 107–128.
Wang, Y.J., Fan, W.M., Zhang, Y., Guo, F., 2003. Structural evolution and $^{40}Ar/^{39}Ar$ dating of the Zanhuang metamorphic domain in the North China Craton: constraints on Paleoproterozoic tectonothermal overprinting. Precam. Res. 122, 159–182.
Wang, Y.J., Fan, W.M., Zhang, H.F., Peng, T.P., 2006. Early Cretaceous gabbroic rocks from the Taihang Mountains: implications for a paleosubduction-related lithospheric mantle beneath the central North China Craton. Lithos 86, 281–302.
Wu, F.Y., Lin, J.Q., Wilde, S.A., Zhang, X.O., Yang, J.H., 2005. Nature and significance of the Early Cretaceous giant igneous event in eastern China. Earth Planet. Sci. Lett. 233, 103–119.
Xu, Y.G., 2001. Thermo-tectonic destruction of the Archean lithospheric keel beneath the Sino-Korean Craton in China: evidence, timing and mechanism. Phys. Chem. Earth (A) 26, 747–757.
Xu, Y.G., 2007. Diachronous lithospheric thinning of the North China Craton and formation of the Daxin'anling–Taihangshan gravity lineament. Lithos. doi:10.1016/j.lithos.2006.09.013.
Xu, Y.G., Bodinier, J.-L., 2004. Contrasting enrichments in high- and low-temperature mantle xenoliths from Nushan, Eastern China: results of a single metasomatic event during lithospheric accretion? J. Petrol. 45, 321–341.
Xu, Y.G., Menzies, M.A., Bodinier, J.L., Bedini, R.M., Vroon, P., Mercier, J.C.C., 1998. Melt percolation-reaction atop a plume: evidence from the poikiloblastic peridotite xenoliths from Boree (Massif Central, France). Contrib. Mineral. Petrol. 132, 65–84.
Xu, Y.G., Chung, S.L., Ma, J.L., Shi, L.B., 2004. Contrasting Cenozoic lithospheric evolution and architecture in the western and eastern Sino-Korean craton: constrains from geochemistry of basalts and mantle xenoliths. J. Geol. 112, 593–605.
Xu, Y.G., Blusztajn, J., Ma, J.L., Suzuki, K., Liu, J.F., Hart, S.R., 2007. Late Archean to Early Proterozoic lithospheric mantle beneath the western North China craton: Sr–Nd–Os isotopes of peridotite xenoliths from Yangyuan and Fansi. Lithos. doi:10.1016/j.lithos.2007.04.005.
Yang, J.H., Wu, F.Y., Wilde, S.A., 2003. A review of the geodynamic setting of large-scale Late Mesozoic gold mineralization in the North China craton: an association with lithospheric thinning. Ore Geol. Rev. 23, 125–152.
Ying, J.F., Zhang, H.F., Kita, N., Morishita, Y., Shimoda, G., 2006. Nature and evolution of Late Cretaceous lithospheric mantle beneath the eastern North China Craton: constraints from petrology and geochemistry of peridotitic xenoliths from Jünan, Shandong Province, China. Earth Planet. Sci. Lett. 244, 622–638.
Zhang, H.F., 2005. Transformation of lithospheric mantle through peridotite–melt reaction: a case of Sino-Korean craton. Earth Planet. Sci. Lett. 237, 768–780.
Zhang, H.F., Sun, M., Zhou, X.H., Fan, W.M., Zhai, M.G., Ying, J.F., 2002. Mesozoic lithosphere destruction beneath the North China Craton: evidence from major-, trace-element and Sr–Nd–Pb isotope studies of Fangcheng basalts. Contrib. Mineral. Petrol. 144, 241–253.
Zhang, H.F., Sun, M., Zhou, X.H., Zhou, M.F., Fan, W.M., Zheng, J.P., 2003. Secular evolution of the lithosphere beneath the eastern North China Craton: evidence from Mesozoic basalts and high-Mg andesites. Geochim. Cosmochim. Acta 67, 4373–4387.
Zhang, H.F., Sun, M., Zhou, M.F., Fan, W.M., Zhou, X.H., Zhai, M.G., 2004. Highly heterogeneous late Mesozoic lithospheric mantle beneath the north China Craton: evidence from Sr–Nd–Pb isotopic systematics of mafic igneous rocks. Geol. Mag. 141, 55–62.
Zhang, H.F., Nakamura, E., Sun, M., Kobayashi, K., Zhang, J., Ying, J.F., Tang, Y.J., Niu, L.F., 2007a. Transformation of subcontinental lithospheric mantle through peridotite–melt reaction: evidence from a highly fertile mantle xenolith from the North China craton. Int. Geol. Rev. 49, 658–679.
Zhang, H.F., Goldstein, S.L., Zhou, X.H., Sun, M., Zheng, J.P., Cai, Y., 2007b. Evolution of subcontinental lithospheric mantle beneath eastern China: Re–Os isotopic evidence from mantle xenoliths in Paleozoic kimberlites and Mesozoic basalts. Contrib. Mineral. Petrol. doi:10.1007/s00410-007-0241-5.
Zhao, G.C., Wilde, S.A., Cawood, P.A., Sun, M., 2001. Archean blocks and their boundaries in the North China Craton: lithological, geochemical, structural and P–T path constraints and tectonic evolution. Precam. Res. 107, 45–73.
Zhao, G.C., Wilde, S.A., Cawood, P.A., Sun, M., 2002. Shrimp U–Pb zircon ages of the Fuping complex: implications for late Archean to Paleoproterozoic accretion and assembly of the North China Craton. American Journal of Science 302, 191–226.
Zhao, X.M., Zhang, H.F., Zhu, X.K., Zhang, W.H., Yang, Y.H., Tang, Y.J., 2007. Metasomatism of Mesozoic and Cenozoic lithospheric mantle beneath the North China Craton: evidence from phlogopite-bearing mantle xenoliths. Acta Petrol. Sin. 23 (6), 1281–1293.
Zheng, J.P., O'Reilly, S.Y., Griffin, W.L., Lu, F.X., Zhang, M., 1998. Nature and evolution of Cenozoic lithospheric mantle beneath Shandong peninsula, Sino-Korean craton, eastern China. Int. Geol. Rev. 40, 471–499.
Zheng, J.P., O'Reilly, S.Y., Griffin, W.L., Lu, F.X., Zhang, M., Pearson, N., 2001. Relict refractory mantle beneath the eastern North China block: significance for lithosphere evolution. Lithos 57, 43–66.
Zheng, J.P., Griffin, W.L., O'Reilly, S.Y., Lu, F.X., Wang, C., Zhang, F., Li, H., 2004. 3.6 Ga lower crust in central China: new evidence on the assembly of the North China Craton. Geology 32, 229–233.
Zheng, J.P., Griffin, W.L., O'Reilly, S.Y., Yang, J.S., Li, T.F., Zhang, M., Zhang, R.Y., Liou, J.G., 2006a. Mineral chemistry of peridotites from Paleozoic, Mesozoic and Cenozoic lithosphere: Constraints on mantle evolution beneath eastern China. J. Petrol. 47, 2233–2256.

Zheng, J.P., Lu, F.X., Griffin, W.L., Yu, C.M., Zhang, R.S., Yuan, X.P., Wu, X.L., 2006b. Lithospheric thinning accompanying mantle lateral spreading, erosion and replacement beneath the eastern part of North China: evidence from peridotites. Earth Sci. Frontiers 13 (2), 76–85.

Zhou, X.H., Armstrong, R.L., 1982. Cenozoic volcanic rocks of eastern China-secular and geographic trends in chemistry and strontium isotopic composition. Earth Planet. Sci. Lett. 58, 301–329.

Zindler, A., Hart, S.R., 1986. Chemical geodynamics. Annu. Rev. Earth Planet. Sci. 14, 493–571.